IOP Publishing Semiconductor Science and Technology
Semicond. Sci. Technol. **34** (2019) 075013 (10pp) https://doi.org/10.1088/1361-6641/ab23b5

Regimes of current transport mechanisms in CdS/CdTe solar cells

H Bayhan[1], E T Dağkaldıran[1], J D Major[2], K Durose[2] and M Bayhan[1]

[1] Department of Physics, Faculty of Science, University of Muğla Sıtkı Koçman, Muğla 48000, Turkey
[2] Stephenson Institute for Renewable Energy/Department of Physics, University of Liverpool, Peach Street, Liverpool, L69 7ZF, United Kingdom

E-mail: hbayhan@mu.edu.tr

Received 25 February 2019, revised 1 May 2019
Accepted for publication 22 May 2019
Published 13 June 2019

Abstract

Forward bias recombination (current transport) mechanisms have been evaluated for thin film solar cells and correlated to the in-gap trap levels present. Here CdTe/CdS devices were chosen as an archetypal example of a modern thin film solar cell, and a set of devices with a range of design variables was used in order to reveal the full range of behaviours that may operate to limit current transport. Experimental current–voltage–temperature datasets were compared to mathematical models of transport, and the in-gap traps were evaluated by thermal admittance spectroscopy. The current transport mechanisms operating are presented on a temperature–voltage diagram. Three regimes were identified: at 'intermediate' voltages, the behaviour was temperature dependent. From 300 K down to 240 K, thermally activated Shockley Read Hall recombination mediated by a 0.38 eV trap (V_{Cd}) dominated the transport. Between 200 and 240 K the transport was thermally activated but below 200 K the mechanism became dominated by tunnel assisted interface recombination. At 'low' voltages (and for all devices at all voltages when measured at $T < 200$ K) band to band recombination is via multi-step tunnelling through in-gap states. At high voltage, the forward current is dominated by the well-known limiting effect of the back Schottky contact to the CdTe which is in reverse bias. The current transport behaviour is also correlated with the n-CdS thickness and $CdCl_2$ processing conditions, both of which are critical to device performance.

Supplementary material for this article is available online

Keywords: CdS/CdTe solar cell, current transport mechanisms, admittance spectroscopy

(Some figures may appear in colour only in the online journal)

1. Introduction

For all but a minority of semiconductor *p–n* junction materials systems, the current flowing in the forward direction is limited to below that expected for an ideal diode (equation (1)) by recombination processes that are energetically preferred to the direct, unimpeded recombination of electrons and holes across the semiconductor band gap. This is indeed the case for the polycrystalline heterojunctions made from low purity semiconductors that are the subject of this paper. For such junctions, a wide variety of alternative recombination pathways may be available, and the mechanisms operating may change with temperature and with the bias voltage applied. Although it is written to describe an ideal diode, equation (1) contains terms that may represent non-ideal behaviour: firstly, the diode factor, n, accounts for deviation from ideality caused by Shockley Read Hall (SRH) recombination through states in the gap (and for which $1 < n < 2$ depending on the position of those states). Secondly, the behaviour of the reverse bias saturation current J_0 may differ from that expected for its ideal thermally activated leakage—if other processes compete with simple thermal excitation over the band gap.

$$J = J_0\left[\exp\left(\frac{qV}{nkT}\right) - 1\right]. \quad (1)$$

Generally, a wide range of physical recombination pathways may operate for any given diode and may dominate in various temperature and voltage regimes. For the cases where the *J–V*:*T* behaviour of these has been described by a mathematical model, fitting of the experimental data to the models allows the physical mechanism of current recombination (i.e. transport over the *p–n* junction) to be evaluated.

Current transport limiting effects in thin film solar cells include both bulk and interface phenomena. In the case of CdTe for example, the forward bias current at relatively high voltages may be limited by an electrical barrier to hole flow between the p-CdTe and the metallic dark side or 'back' contact. The highly mismatched CdTe/CdS hetero-interface may also play a part, with the recombination rate perhaps being limited by the interface recombination velocity, or the supply of carriers to it, or else itself be influenced by tunnelling. Trap-mediated SRH recombination may operate in the bulk and may be augmented by a contribution from in-band tunnelling. Finally, as an alternative to direct recombination over the gap, or to SRH recombination, the band to band recombination pathway may be entirely negotiated by multi-step tunnelling. Further details of these mechanisms—and of the functional forms of their behaviours that may be used to identify them in practice follow below.

The materials and diodes considered here were solar cells comprising CdTe/CdS. This is an archetypal thin film polycrystalline solar cell, for which the CdTe is p-type and comprises the absorber, and the CdS is n-type, and acts as a window layer. In order to expose the full range of physical current transport effects operating, a matrix of devices was fabricated having CdS thicknesses in the range 60–240 nm and $CdCl_2$ processing times (heat treatment) for between 10 and 40 min. Although the physical effects of processing with $CdCl_2$ and the thickness of CdTe layer on CdTe solar cells were investigated extensively [1], there has not been, however, a comparative study to understand the relative influences of the CdS layer thickness and the processing duration onto the improvement of the cell conversion efficiency linked with loss mechanisms at hetero- interface.

Both of these variables are known to introduce changes to the materials that could affect the behaviour of the solar cells and their current transport mechanisms. For example, the heat-treatment with $CdCl_2$ is known to be essential in order to obtain working devices, and it is known to be associated with a change in transport mechanism from multi-step tunnelling to thermally activated nature [2]. Moreover, such heat treatment is known to promote inter diffusion between the CdS and the CdTe which could affect the viability of interface recombination [3]. Since absorption in the CdS window layer does not contribute to the photocurrent, its thickness also has a profound effect on solar cell performance. Finally, the window layer type has been shown to influence the deep levels present in the absorber, with CdS, ZnS and ZnSe all giving different behaviours [4]. As its thickness is understood to also influence the electrical junction [5], this confirmed the selection of the CdS thickness as an experimental variable in the present work.

In this work we compare experimental current–voltage behaviours with a variety of physical current transport models in order to identify both the mechanisms operating and the regimes of voltage and temperature over which they apply. In addition, we use a spectroscopic method—thermal admittance spectroscopy (TAS)—in order to identify the deep and shallow levels present in the materials that may determine the mechanisms of current transport that operate.

Overall, we demonstrated 'low', 'medium' and 'high' voltage regimes for current transport in forward bias in the dark. At 'high' voltages, $V > V_{oc}$, the current is limited by the dark side 'back contact' hole barrier, as usual. In the 'intermediate' regime, $0.3 < V(V) < 0.6$ the behaviour is temperature dependent: at normal solar cell operating temperatures, it is bulk SRH limited, while below 240 K a thermal contribution persists, but transport is now by tunnelling assisted interface recombination at the CdS/CdTe interface. For 'low' voltages, $0 < V\,(V) < 0.1$–0.3, and in any case for all curves at all voltages when measured below 200 K, the current transport is dominated by multi-step tunnelling for all samples.

2. Current limiting mechanisms invoked in this work

The following is a description of the forward current limiting recombination mechanisms ('current transport mechanisms') that are invoked here in the interpretation of the experimental results of *J–V*:*T* and thermal admittance spectroscopy in this work. As a starting point for the evaluation of *J–V*:*T* data sets, equation (1) is approximated for forward bias conditions (i.e. $\exp[qV/nkT] \gg 1$), and the term J_0 is expressed as a thermally activated quantity with activation energy E_A, i.e. $J_0 = J_{00}\exp\left(\frac{-E_A}{nkT}\right)$, giving equation (2) for the recombination current:

$$J = J_{00}\exp\left(\frac{-E_A}{nkT}\right)\exp\left(\frac{qV}{nkT}\right). \tag{2}$$

Since a single value of J_0 may be extracted from each *J–V* curve, a log plot allows the temperature range over which any thermally activated behaviour is present to be identified, and the thermal activation energy E_A to be estimated. Both SRH and interface recombination mechanisms are usually thermally activated and would be expected to be represented by such an activation energy.

2.1. Hole barriers at the contacts to p-CdTe ('roll over')

Since CdTe has a very high electron affinity (4.5 eV), and it is p-type, the resulting value of the electron affinity plus the band gap (5.95 eV) must be exceeded by the work function of the contact metal in order to achieve an Ohmic contact [6, 7]. No metal has a work function higher than this and so all contacts to p-CdTe have a built-in barrier to majority carrier flow, i.e. a hole barrier. This barrier depresses the forward bias current, and causes 'roll over' of the *J–V* curve shape at high forward bias [8]. This current limiting effect is frequently expressed by thermionic emission [9]. Recently

Bayhan *et al* [10], has also demonstrated that classical Schottky-type conduction with pronounced effect of interfacial defect states can be proposed for the dominating reverse route at reverse biased back contact interface. Nevertheless, if the barrier height is less than about 0.5 eV it does not affect the *J*–*V* curve shape below V_{oc}, and hence is of no consequence for solar cell operation [8, 11]. We observed this behaviour in all cells studied here, but since it is already well known it is not a main theme of this work.

2.2. SRH recombination in the bulk of the depletion region

2.2.1. Thermally activated SRH recombination. Thermally activated SRH recombination is one of the best-known recombination/current transport mechanisms, in which electrons and holes recombine via in-gap states located in the space charge region (SCR) [12]. For the case of uniformly distributed traps, SRH recombination may be identified from experimental *J*–*V*: *T* datasets by plotting $\ln(J_0\ T^{-2.5})$ versus $1/T$ which yields an activation energy of $E_A = E_g/n$, where *n* is the diode factor [13]. For an example using $CuInSe_2$ thin film solar cells, see [14].

Recombination through interface states (rather than distributed in the SCR), is described by an extension of the SHR formalism. In general, if $E_A < E_g/n$, $E_A = V_{bi}$ and the value of J_0 is higher than expected, then these are indicators that interface recombination is highly likely [15].

For the SRH theory *n* takes the values $1 < n < 2$, with an ideal diode having $n = 1$, and mid-gap traps giving $n = 2$. However, for the case of thin film solar cell materials, values of $n > 2$ are reported for SRH recombination, although the value of *n* no longer carriers the same physical meaning in such cases.

Rau [16] examined the case of SRH recombination mediated by band tails rather than discrete in-gap traps. (This is an appropriate model for CIGS and other multernary alloys for which alloy disorder gives band tails). The energy distribution of traps in the tails was described by an exponential density, $dN(\eta)\ \alpha\ \exp(-\eta/kT*)d\eta$, where $\eta = (E_T–E_V)$, the energy difference from the band edge, and the width of the distribution in the band tail being described by the energy $kT*$. For this case the analysis in [15] yields a current–voltage relation that is described by equation (3)—in which E_g is the band gap. This applies to the 'intermediate' voltage regime described in the results section of the present work.

$$J = J_{00}\exp\left(\frac{-E_g}{nkT}\right)\exp\left(\frac{qV}{nkT}\right). \tag{3}$$

Furthermore, Rau [16] demonstrated that the diode factor for this case has the temperature dependence in equation (4), and for which $T*$ is related to the band tail width as above.

$$\frac{1}{n} = \frac{1}{2}\left[1 + \frac{T}{T^*}\right]. \tag{4}$$

The functional form of equation (3) is similar to that for other current transport models and so replotting the experimental data using this equation may be insufficient to identify the exact mechanism operating. Hence evaluation of the temperature dependence of *n* may also be valuable—for example using equation (4) above or equation (5) below.

2.2.2. SRH with band tails and a contribution from tunnelling. Rau [16] went on to evaluate the case of SRH recombination via states contained in the same type of band tails as above, but with a contribution from tunnelling. Here the recombination centres are accessed from the bands either partly or wholly by tunnelling. The current–voltage relation could be described by an equation like equation (3)—and plots of *n* $\ln J_0$ versus E_g/kT should be linear for this mechanism also. However, the diode factor variation with temperature given with equation (5), now contains two terms: E_{00} - this being energy related to the tunnelling step; and T^* as before. In equation (5), where $T^* \to \infty$, the expression describes pure tunnelling, while when $E_{00} = 0$, it is for the purely thermally activated SRH process as above.

$$\frac{1}{n} = \frac{1}{2}\left[1 - \frac{{E_{00}}^2}{3(kT)^2} + \frac{T}{T^*}\right]. \tag{5}$$

In this work we found evidence that SRH mechanisms dominate the current transport at room temperature and at 'intermediate' voltages.

2.3. Interface dominated recombination

When interface recombination dominates, the product of the diode factor and the thermal activation energy for the reverse bias saturation current, J_0 is expected to equal the diffusion (built in) potential i.e. $nE_A = V_{bi}$, [7]. Further to this, the rate determining step may be either the interface recombination rate itself or the supply rate of holes to the interface [14]. For interface limited recombination, $\ln J_0$ versus $1/T$ is expected to be linear, while for supply limited recombination $\ln(J_0T^2)$ versus $1/T$ is expected to be linear. In both cases Yoo [14] gives a refinement to the activation energy $E_A = V_D–\delta_p$, where V_D is the diffusion potential (built-in potential, V_{bi} above), and δ_p is the energy difference between the valence band edge and the Fermi level.

For the case where tunnelling influences the arrival of carriers at the interface, Nadenau [17] evaluated the *J*–*V* relation as equation (5), and the variation of the diode factor with temperature as equation (7)

$$J = J_{00}\exp\left(\frac{\varphi_b^f}{nkT}\right)\exp\left(\frac{qV}{nkT}\right), \tag{6}$$

where φ_b^f/α is the flat band barrier height and where α is a function of the dielectric constants and depletion widths on both sides of the junction:

$$\alpha = \frac{w_p/\varepsilon_p}{w_p/\varepsilon_p + w_n/\varepsilon_n}, \tag{7}$$

$$n = \frac{1}{\alpha}\frac{E_{oo}}{kT}\cot h\left(\frac{E_{oo}}{kT}\right). \quad (8)$$

In this work we found that interface-dominated recombination controls the forward bias current flow for all samples in the 'intermediate' forward bias voltage region at temperatures below 240 K. However, below ~200 K a different mechanism operates—multi-step tunnelling.

2.4. Multi-step tunnelling from band to band

In this case electrons first stepwise tunnel from the conduction band of n-CdS layer into the empty states located in the p-CdTe layer and subsequently recombine through a staircase of closely spaced interfacial states in the depletion region. Since tunnelling originates between the bottom of the conduction band in n-type material and the top of valence band in p-type CdTe layer the forward current can be given as [18],

$$J = \beta N_t \exp\left(\frac{-\alpha R {E_t}^{3/2}}{(V_d - V)^{1/2}}\right), \quad (9)$$

where R is the number of tunnelling steps, V_d is the diffusion voltage and β is a constant and each state associated with an energy difference E_t. For this mechanism, n varies strongly with T and q/nkT is a constant.

We observed multistep tunnelling in all our samples at $T < 200$ K at all voltages, and for all samples in the 'low' voltage range at all temperatures.

3. Thermal admittance spectroscopy methodology

Here we used the thermal admittance spectroscopy method to evaluate the energies and densities of traps in the solar cell devices—the method is now summarised:

Electronically active trapping levels locating in the depletion region of a typical n^+p junction contribute to its admittance at lower frequencies and/or higher temperatures. In the presence of an ideal discrete majority trap level with density N_T, the junction capacitance can be expressed as [19],

$$C(\omega) = C_{\rm SCR} + \frac{C_{lf} - C_{\rm SCR}}{1 + \omega^2\tau^{*2}}, \quad (10)$$

where $\omega = 2\pi f$, $C_{\rm SCR} = \frac{\varepsilon_r q N_A}{2V_{bi}}$ is the geometric capacitance, C_{lf} is the low frequency capacitance which depends on N_T and acceptor concentration, N_A and $\tau^* = 1/\omega_O$ is the time constant of a trap level. The inflection frequency ω_O of the transition can be related to the emission rate e_T of the dominating trapping level in the case of small trap concentration, $N_T \ll N_A$ as [20, 21],

$$\omega_O = 2e_T(T);\ \omega_o(T) = 2N_V v_{\rm th}\sigma_p \exp\left(-\frac{E_T}{kT}\right) = 2\xi_o T^2 \exp\left(-\frac{E_T}{kT}\right), \quad (11)$$

where σ_p is the capture cross-section for holes, $v_{\rm th}$ is the thermal velocity, N_V is the effective density of states in the valence band and E_T is the activation energy of the defect with respect to the corresponding band edge. All the temperature independent parameters are included in the emission factor ξ_o. The values of ω_O at different temperatures were estimated from maxima in the derivative $-f{\rm d}C/{\rm d}f$ versus f variation [22]. An Arrhenius plot may be used to estimate the values of activation energy of the dominating trapping level, E_T and the corresponding ξ_0 from the slope of the observed linearly varying and the intercept on y-axis, respectively. Since occupation of the trap level follows the applied ac signal, the distribution of defect density in energy $N_T(E)$ can also be estimated [22] as,

$$N_T(E_\omega) = c(E_\omega)\frac{1}{kT}\frac{{\rm d}C(\omega)}{{\rm dln}\omega}, \quad (12)$$

where $C(E_\omega)$ denotes the contribution of defects which depends on their energetic depth and on the band diagram of the pn junction. The frequency axis is converted into energy axis by using $E_\omega = kT{\rm ln}\left(\frac{2\xi_o T^2}{\omega}\right)$ to yield $N_T(E_{\rm A})$ versus $E_{\rm A}$ spectra.

4. Experimental

Solar cells having the structure Au/CdTe/CdS/ZnO/FTO/glass were prepared as described below, with the FTO/glass being commercial NSG Ltd 'TEC 10' SnO_2:F coated glass. The ZnO (100 nm) was deposited by reactive RF sputtering from a Zn target in the presence of oxygen. CdS window layers having thicknesses of 60, 120 or 240 nm were then deposited by RF sputtering from a CdS target in Ar and at a power of 60 W with the substrate temperature being 200 °C. All sputtering was conducted in an AJA International Inc. system. The CdTe absorbers were deposited by close space sublimation in a system manufactured by Electro-Gas Systems Ltd, UK with the source being held at 615 °C and the substrate at 520 °C. To enhance the in-diffusion of $CdCl_2$, the as-grown samples were first etched in a nitric-phosphoric acid mixture for 15 s to create a Te-rich surface prior to chloride treatment [23]. The CdTe surfaces were then coated with $CdCl_2$ before annealing in air for 10, 20 or 40 min at 430°C. The device structures were completed by the evaporation of arrays of nine Au 0.25 cm^2 back contacts to the CdTe.

A total of nine solar cell structure types were made as described above, and these will be referred to by sample numbers that include the CdS thickness (60, 120, 240 nm) and the processing time (10, 20, 40 min). For example, 'Cell 120/40' contains 120 nm of CdS and was $CdCl_2$ treated for 40 min.

External quantum efficiency (EQE) measurements were made using a Bentham PVE300 system at room temperature. The temperature dependent dark current density–voltage (J–V:T) and dark admittance spectroscopy (C–f:T) measurements were conducted using a computer controlled Keithley source meter and a Solatron 1260 frequency response analyser—with a Janis closed cycle cryostat in the temperature range $70 > T\,({\rm K}) > 330$.

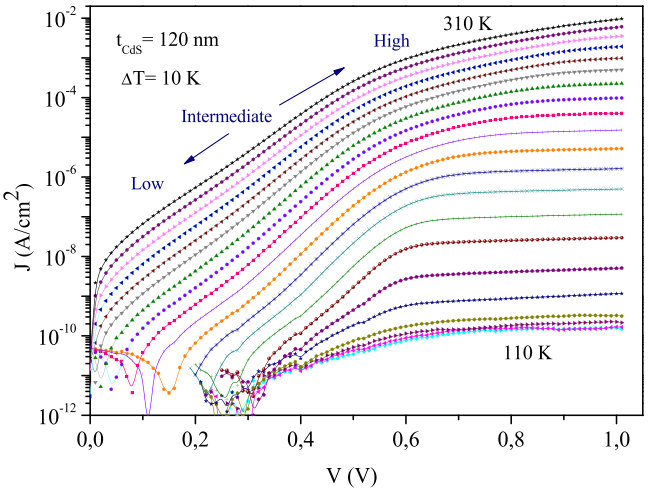

Figure 1. Log plot of dark forward bias *J–V*:*T* data for CdS/CdTe Cell120/20, the highest efficiency device from the study. The curves show behaviour that is typical for most of the devices studied: there is 'roll over' contact limitation to the current at the relatively 'high' voltages. Curves in the 'intermediate' voltage range show complex temperature dependent behaviour discussed in the text. At 'low' voltages, and for all data recorded below 200 K, there is a separate current transport regime.

5. Results and discussion

5.1. EQE and interdiffusion

The external quantum efficiency curves of all cell types are shown in figure S1 in the supplementary information. Since the PV results are not the main theme of the current work they will be described very briefly.

Generally, the use of increasingly thick CdS caused the current harvested to be decreased due to the parasitic absorption in the CdS that does not contribute to photocurrent. This is clearly shown in the EQE spectra, which are increasingly depressed in the CdS absorption region as the thickness of CdS is increased—a well-known result [24]. The chloride treatment also gave the expected result of having an optimum duration for maximum performance, this being for 20 min treatment in all cases. Since the CdS/CdTe couple is known to inter-diffuse both ways, the EQE data was replotted (not shown—see supplementary information and [25–27] for the method) to estimate the band gaps and hence compositions of the inter-diffused regions. These were interpreted as compositions using the Vegard relations $E_g(x) = 1.74x^2 - 1.01x + 1.51$ eV [24] and $E_g(y) = 2.4\,y + 1.51(1-y) - 1.8(1-y)$ eV [28] for $CdTe_{1-x}S_x$ and CdS_yTe_{1-y} solid solutions respectively. However, the results (0.040–0.058 for the S fraction in CdTe and 0.012–0.025 for the Te fraction in CdS) given in table S1 do not indicate any systematic dependence on either the thickness of CdS or the annealing time, (i.e. the amount of material available to diffuse or the driver for diffusion).

5.2. Current transport in the dark

As a starting point for the analysis, log plots of all the temperature dependent *J–V* data were prepared, with the example for Cell 120/20 being shown in figure 1, this being typical. The behaviour of the curves may be divided into three distinct regions identified as follows: a 'high' voltage region with $V > \sim 0.6$ V; an 'intermediate' region—for $V < \sim 0.6$ V, but lying to the right of the line connecting $V = 0.4$ V to $J \approx 10^{-8}$ mA cm^{-2} and a 'low' voltage region which contains all data to the left of the line connecting $V = 0.4$ V to $J \approx 10^{-8}$ mA cm^{-2}, along with all data below 200 K.

5.2.1. 'High' voltage region. The 'high' voltage behaviour may be dealt with trivially—the forward bias current limitation seen here is caused by the back-contact barrier to the CdTe, and well-known as 'roll over'. When the temperature exceeds room temperature, this barrier may be overcome thermally, and it no longer limits the current [29].

5.2.2. 'Intermediate' voltage region. This region is more complex and shows temperature dependent changes. We used both activation energy plots of the reverse bias saturation current and plots of n_2 versus temperature in order to evaluate the current transport in this region, as shown in figures 2–5 for the highest performing cell for each of the three thicknesses of CdS tested. For each device, both the Arrhenius and plots of $\ln(J_0\ T^{-2.5})$ versus $1/T$ were linear from room temperature down to about 180–200 K (implying SRH recombination), whereas the $n(T)$ graphs showed a distinct discontinuity at around 240 K. The activation energies for the thermal processes and the functional forms of the $n(T)$ behaviour are now compared with the models and tests from section 2 in order to deduce the current transport mechanisms.

Table 1 shows the activation energies extracted from both the Arrhenius plots in figures 2–4 and the plots of $\ln(J_0\ T^{-2.5})$ versus $1/T$ (not shown) for each device in the range ~200–300 K. Those from $\ln(J_0\ T^{-2.5})$ fall in the range 0.44–0.64 eV and would be expected to give $E_A = E_g/n$ if the model applies. Here, n takes values of up to 2 (figures 2–5) and so the minimum values expected from the model should be $E_g/2$, which is 0.725 eV for CdTe. Since actual activation energies measured fall very short of this value, they do not unambiguously support bulk SRH recombination through discrete levels. Often in the literature, failure of this model of bulk recombination is taken to imply that there is interface recombination. For the alternative case of interface recombination, the product $nE_A = V_{bi}$, the built-in voltage [15], which for CdTe is 1.18 eV. Comparison with the experimental values in table 1, shows that most are rather lower than expected for this model, with only two of the values (for Cell 120/20–1.102 eV, and Cell 240/10–1.13 eV) being comparable that expected.

Despite giving clear evidence of some kind of thermally activated recombination process, the comparison of the thermal activation energies for curves above 200 K does not on its own give any clear indication of whether bulk (SRH) or interface recombination is operating, even though those are

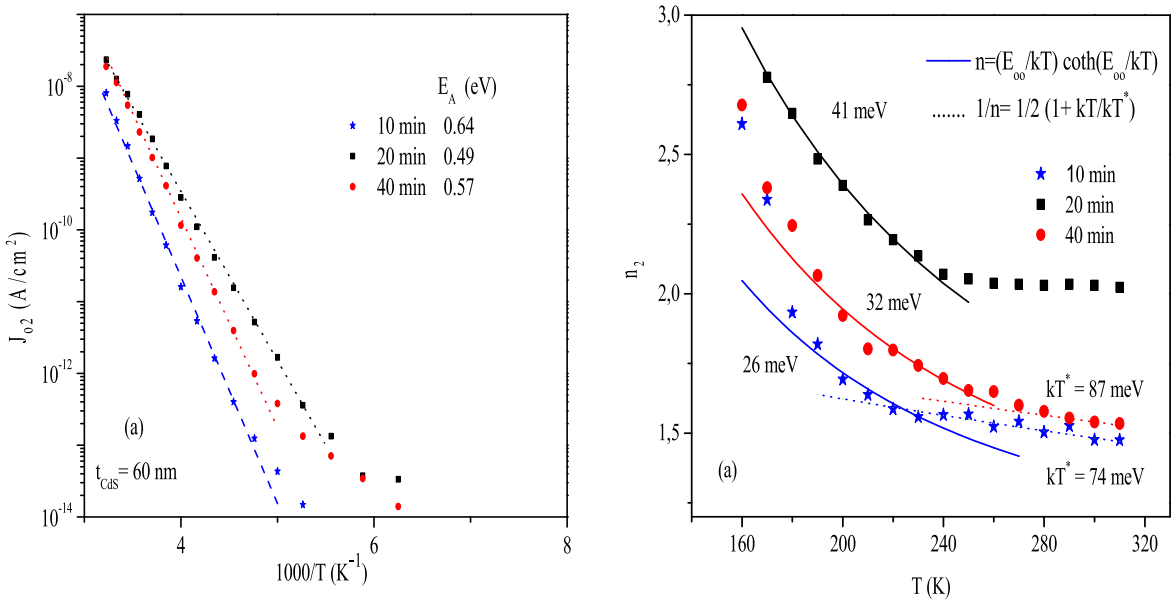

Figure 2. Plots of (a) log J_{02} versus $1/T$ and (b) n_2 versus T for CdTe/CdS solar cells having 60 nm of CdS and processed for 10, 20 and 40 min J_0 shows thermally activated behaviour down to 180–200 K. In (b) fit lines are shown below 240 K for $n(T)$ for the case of tunnelling assisted interface recombination. Above 240 K, $n(T)$ for two of the devices could be fitted using the model for SRH recombination through a continuous distribution of band-tail states—even though in practice this sample has discrete shallow, rather than distributed in-gap states. See section 3.3 for discussion.

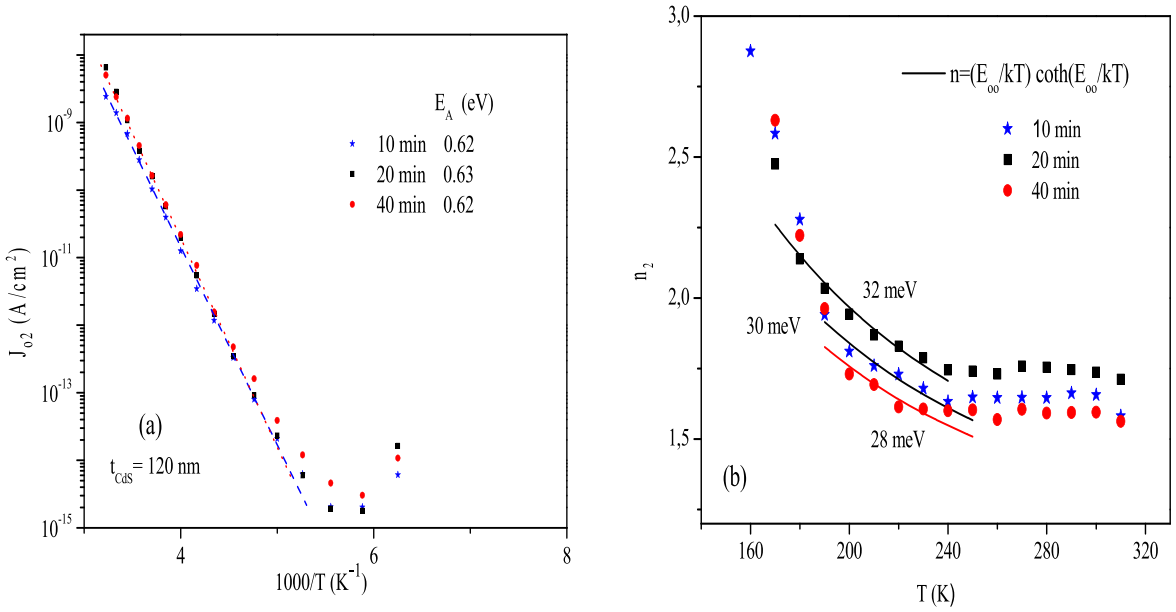

Figure 3. Plots of (a) log J_{02} versus $1/T$ and (b) n_2 versus T for CdTe/CdS solar cells having 120 nm of CdS and processed for 10, 20 and 40 min. As for the other devices, thermally activated processes dominate the reverse bias saturation current behaviour down to ~200 K. Fits to $n(T)$ for tunnelling assisted interface recombination are good for $200 < T < 240$ K.

the most likely thermally activated processes. Hence further evidence is sought from the behaviour of the diode ideality factors and their temperature dependencies.

Above 240 K the experimental values of n are independent of T, or else show only weak temperature dependence. Equation (4) is for the most likely model to fit of those presented in section 2, and fits were attempted for all curves as shown in figures 2(b)–4(b). Of these, most did not give a good fit to equation (4), and it was a better approximation to assume that n is independent of T. However, there were two exceptions, for Cells 60/10 and 60/40: for these a good fit was obtained using characteristic energies kT^* of 74 and 87 meV respectively—these being the energies that define the widths of the exponential band tails through which SRH recombination takes place in Rau's model [16]. This fit is spurious, as discussed in section 3.3 with reference to the trap energies measured for these cells.

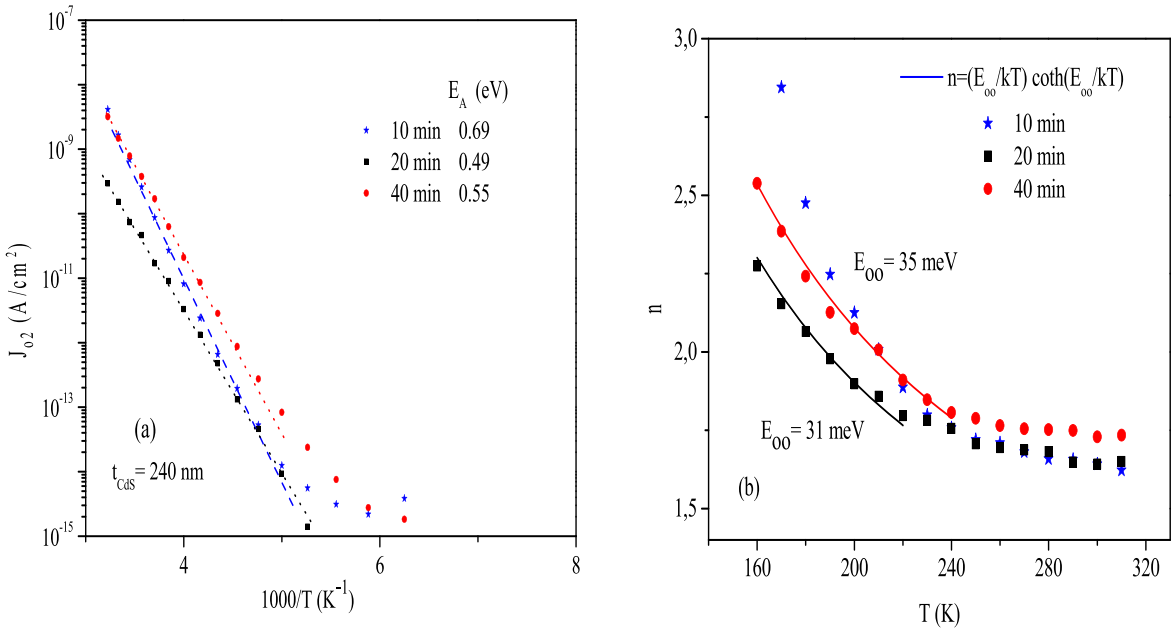

Figure 4. Plots of (a) log J_{02} versus $1/T$ and (b) n_2 versus T for CdTe/CdS solar cells having 120 nm of CdS and processed for 10, 20 and 40 min. Again, thermally activated processes dominate the reverse bias saturation current behaviour down to ~200 K and fits to $n(T)$ for tunnelling assisted interface recombination are good for $200 < T < 240$ K.

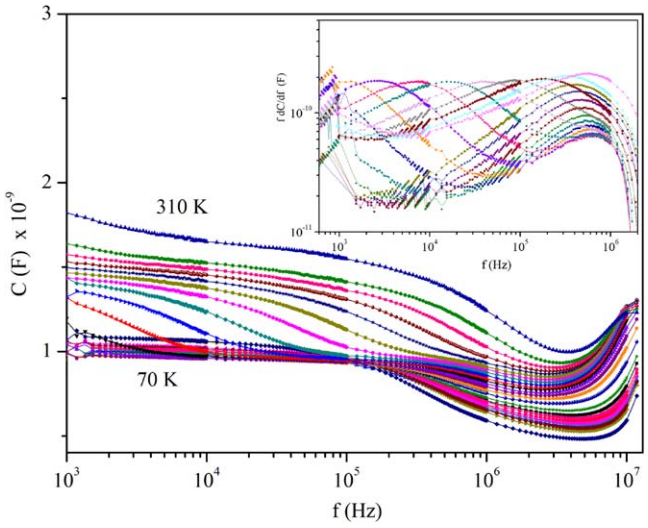

Figure 5. The temperature dependent *C–f* characteristics for Cell 120/20. The inset shows the differential spectra at temperatures between 70 and 310 K.

In the temperature range $200 < T < 240$ K, the experimental diode factors for all the cells vary very strongly with T, increasing smoothly with decreasing temperature. Fitting to equation (8), for the case of tunnelling enhanced interface-dominated recombination [16], was successful for all curves, and the fitting parameters E_{00}, extracted are shown in table 1. This fit indicates that the tunnelling enhanced interface recombination mechanism is likely to be dominant in the range 200–240 K in the intermediate voltage region. However, since the activation energy plots gave straight lines that persist down to 200 K, this is evidence to the continued thermal contribution to the tunnelling enhanced interface recombination.

5.2.3. 'Low' voltage region. At low voltages and in any case for $T < 200$ K, the log *J–V* curves show different behaviour: n is temperature dependent but diverges from the fits tested above and shown with lines on figures 2–5. Also, q/nkT is a constant. These are characteristics of multi-step tunnelling which has been reported before for CdTe/CdS solar cells [10].

5.3. Analysis of C–f characteristics

A summary of the thermal admittance spectroscopy method used was presented in section 2. Figure 5 shows the frequency dependence of junction capacitance between 70 and 320 K for the highest efficiency device Cell120/20, its features being typical of all those measured. The capacitance decreases as the frequency increases and increases with temperature representing the thermal activation onset of individual processes having emission rates limiting the capacitance of the solar cell. The values of ω_0 (equation (10)) at different temperatures were estimated from maxima in the derivative $-f\mathrm{d}C/\mathrm{d}f$ versus f curve as shown in the inset of figure 5 [19]. Figure 6 illustrates the Arrhenius plot used to estimate the values of activation energy of the dominating trapping level, E_T and the corresponding ξ_0 values. The density of trapping states, $N_T(E_A)$ versus E_A, is shown in the inset of figure 6. The activation energies and densities of trap states extracted this way are summarized in table 1 for all samples.

The traps identified were as follows:

(i) 0.38 eV having a density of 3.5–6.5 $\times$ 10^{14} eV^{-1} cm^{-3}. This appears in all but two of the samples and is evident in the temperature range $190 < T$ (K) < 290. Traps of this energy are often attributed to V_{Cd} [30].

Table 1. Parameters extracted from the *J–V*:*T* and thermal admittance data for all CdTe/CdS solar cells in the study. Activation energies for J_0 are given for both Arrhenius and $\ln(J_0\,T^{-2.5})$ versus $1/T$ plots. Parameters extracted from fitting $n(T)$ in the two main temperature ranges are listed. The trap energies and densities are from thermal admittance spectroscopy. The data is discussed in the text.

	$J_0(T)$ $T >$ 180–200 K		$n(T)$ 200 $< T <$ 240 K	$n(T)$ $T >$ 240 K	Trap energies and densities	
Sample number CdS thickness (nm)/processing time (mins)	nE_A (eV) Arrhenius plot	E_A (eV) SRH single trap model [13]	E_{00} (meV) for from interface recombination model	$kT*$ (meV) from band tail SRH recombination model [15]	E_t (eV)	N_t ($eV^{-1}cm^{-3}$)
Cell 60/10	0.94	0.63	26	74	0.08	1.0×10^{15}
Cell 60/20	0.99	0.63	41	no fit	0.38	3.5×10^{14}
Cell 60/40	0.97	0.48	32	87	0.09	1.0×10^{15}
Cell 120/10	1.023	0.64	32	no fit	>0.02	1.0×10^{15}
				no fit	0.15	7.0×10^{14}
				no fit	0.38	6.0×10^{14}
Cell 120/20	1.02	0.64	30	no fit	0.38	6.5×10^{14}
Cell 120/40	1.003	0.62	28	no fit	0.38	4.1×10^{14}
Cell 240/10	1.13	0.62	35	no fit	0.38	4.7×10^{14}
Cell 240/20	0.75	0.44	31	no fit	0.38	3.5×10^{14}
				no fit	>0.02	1.6×10^{15}
Cell 240/40	0.88	0.55	35	no fit	0.38	4.2×10^{14}

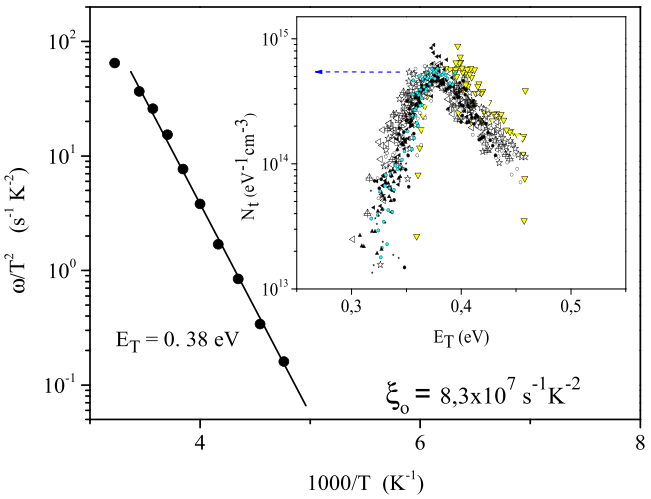

Figure 6. Arrhenius plot of the frequency response data for the most commonly observed in-gap defect state seen in this study, at 0.38 eV. The inset shows the distribution for the corresponding density of trap states. This data is for the most efficient device from the trial, Cell 120/20, having 120 nm of CdS and processed with $CdCl_2$ for 20 min.

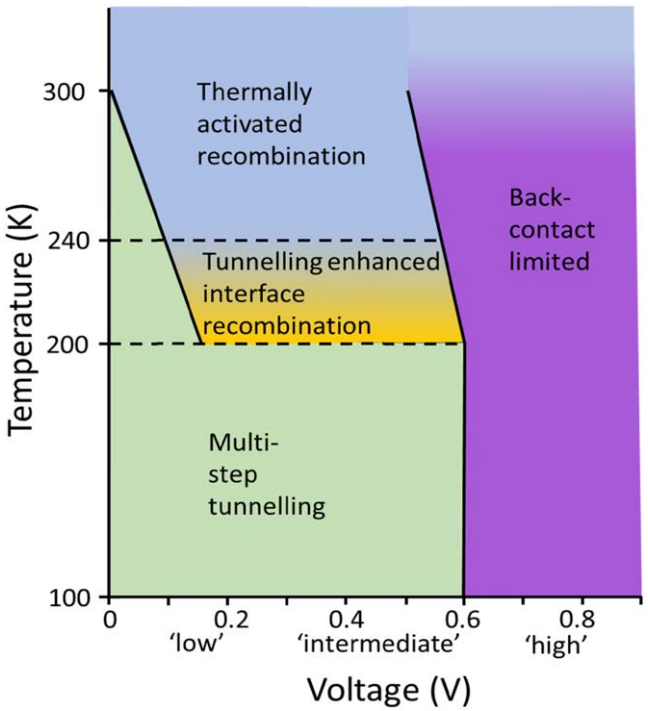

Figure 7. Summary of the current transport regimes identified in this work for CdTe/CdS solar cell devices on the *T–V* plane. Arrhenius plots of J_0 show thermally activated behaviour down to 200 K. Evaluation of the temperature dependence of n shows the onset of tunnelling enhanced interface recombination below 240 K, and it dominates down to 200 K when multi-step tunnelling from band to band takes over. Above V_{oc}, the back-contact hole barrier limits the forward bias current until the temperature is sufficiently high for thermal excitation to overcome it.

(ii) 0.15 eV having a density of $7 \times 10^{14}\,eV^{-1}\,cm^{-3}$ and appearing in the temperature range $270 < T\,(K) < 310$. This trap appears in two samples, Cells 60/40 and 120/10.

(iii) 0.08–0.09 eV having a density of $10^{15}\,eV^{-1}\,cm^{-3}$, this trap appears at $220 < T\,(K) < 280$ in two samples, Cells 60/10 and 60/40. These are the only samples that gave a good fit to the $n(T)$ relation for SRH recombination through band tails (equation (4)), but the model is physically inappropriate (see below).

(iv) $E_T < 0.02$ eV, having densities in the range 3.5×10^{14}–$1.5 \times 10^{15}\,eV^{-1}\,cm^{-3}$, this shallow trap appears in the temperature range $80 < T\,(K) < 200$.

Of these, the trap at 0.38 eV (the most pervasive in the cells here) is a well-known defect. The temperature range over which it is observed ($190 < T\,(K) < 290$) is consistent with the range of thermally activated recombination

behaviour seen in the Arrhenius plots (figures 2–4) and the plots of $\ln(J_0T^{-2.5})$ versus $1/T$. It is therefore likely that this (relatively deep) trap is implicated in the thermally activated recombination process, and that the recombination mechanism in this range is SRH through this defect.

As noted in (i) above, those two samples having discrete defect levels at 0.08–0.09 eV and identified in the spectroscopy in this paper are the same two that give a good fit to the $n(T)$ relation for SRH recombination through states distributed in band tails, equation (4) [15]. Moreover, the characteristic energies that describe the exponential the tail breadth, kT^*, obtained from the fits (in figure 2(b)) are 0.074 and 0.087 eV. While at first sight these are comparable to the trap energies, this is a coincidence: While the spectroscopy has identified discrete levels, Rau's model is for SRH recombination through band tails i.e. a continuous distribution of levels. Since the measured discrete level peak lies under the near band edge part of the exponential band tail for the fit, this has allowed the fit to be made for a physically different situation from the one that it was intended for. Moreover, while the material for which the model was devised, CIGS, can have alloy disorder and hence band tails, CdTe, as a binary material does not suffer from band tailing from alloy disorder.

6. Conclusion

Regimes of forward bias current transport mechanisms (recombination currents) in CdTe/CdS solar cells have been evaluated by comparing models with experimental J–V:T data and further informed by determining the in-gap defects present using thermal admittance spectroscopy. A range of n-CdS window layer thicknesses and $CdCl_2$ processing times were used to expose all of the important transport mechanisms that may be influenced by these variables. Figure 7 summarises the main findings.

Three regimes of forward bias behaviour were identified. At 'low' voltages, and also below 200 K for other voltages up to $\sim V_{oc}$, multi-step tunnelling from band to band dominates the flow of current through the junction. In the 'intermediate' range, there is temperature-dependent behaviour: from room temperature down to 200 K, recombination is thermally activated. Down to 240 K the most likely mechanism is SRH recombination through a V_{Cd} defect at 0.38 eV identified by thermal admittance spectroscopy in the same temperature range. Below 240 K and above 200 K, the thermal contribution persists, but now the recombination takes place at the CdS-CdTe interface and there is a contribution from tunnelling. (Fitting of the $n(T)$ behaviour for samples having discrete shallow levels—using the model appropriate for SRH through a distribution of states in band tails—can give an apparently good fit, despite it being an inappropriate physical model).

A little above V_{oc}, the forward current in the main junction is limited by the back-contact junction which is now in reverse bias, the so-called rollover effect seen in J–V curves for CdTe solar cells. Since the hole barrier responsible is low, typically < 0.5 eV, elevation to moderate temperatures overcomes this barrier allowing the device to assume thermally activated current characteristics again.

Acknowledgments

The authors acknowledge part funding through EPSRC grants EP/P02484X/1 and EP/K005901/1

ORCID iDs

H Bayhan https://orcid.org/0000-0001-7792-0305
J D Major https://orcid.org/0000-0002-5554-1985
K Durose https://orcid.org/0000-0003-1183-3211

References

[1] Bosio A, Rosa G and Romeo N 2018 Past, present and future of the thin film CdTe/CdS solar *Cells Solar Energy* **175** 31–43
[2] Al-Allak H M, Brinkman A W, Richter H and Bonnet D 1996 Dependence of CdS/CdTe thin film solar cell characteristics on the processing conditions *J. Crystal Growth* **159** 910–5
[3] Taylor A A, Major J D, Kartopu G, Lamb D, Duenowe J, Dhere R G, Maeder X, Irvine S J C, Durose K and Mendis B G 2015 A comparative study of microstructural stability and sulphur diffusion in CdS/CdTe photovoltaic devices *Sol. Energy Mater. Sol. Cells* **141** 341–9
[4] Fedorenko Y G, Major J D, Pressman A, Phillips L J and Durose K 2015 Modification of electron states in CdTe absorber due to a buffer layer in CdTe/CdS solar cells *J. Appl. Phys.* **118** 165705
[5] Roussillon Y, Giolando D M, Karpov V G, Shvydka D and Compaan A D 2004 Reach-through band bending in semiconductor thin films *Appl. Phys. Lett.* **85** 3617–9
[6] Brinkman A W 1994 in EMIS Datareview Series Vol 10: Properties of Narrow Gap Cadmium-based Compounds, Capper P (Ed.) IET (https://doi.org/10.1002/crat.2170300311)
[7] Fahrenbruch A L 1987 Ohmic contacts and doping of CdTe *Sol. Cells* **21** 399–412
[8] Stollwerck G and Sites J R 1995 *Proc. 13th European PVSEC* pp 2020–3
[9] Demtsu S H and Sites J R 2006 Effect of back-contact barrier on thin-film CdTe solar cells *Thin Solid Films* **510** 320–4
[10] Bayhan H, Özden S, Major J D, Bayhan M, Dağkaldıran E T and Durose K 2016 A comparison of the effect of $CdCl_2$ and $MgCl_2$ processing on the transport properties of n-CdS/p-CdTe solar cells and a simple approach to determine their back contact barrier height *Sol. Energy* **140** 66–72
[11] Niemegeers A and Burgelman M 1997 Effects of the Au/CdTe back contact on IV and CV characteristics of Au/CdTe/CdS/TCO solar cells *J. Appl. Phys.* **81** 2881
[12] See for example Goetzberger A, Knobloch J and Voss B 1998 *Crystalline Silicon Solar Cells.* (Chichester: Wiley)
[13] Sah C, Noyce R N and Shockley W 1957 Carrier generation and recombination in p–n junctions and p–n junction characteristics *Proc. IRE* **45** 1228–43 *Sept.*
[14] Yoo J B, Fahrenbruch A L and Bube R H 1990 Transport mechanisms in ZnO/CdS/$CuInSe_2$ solar cells *J. Appl. Phys.* **68** 4694–9

[15] Fahrenbruch A L and Bube R H 1983 *Fundamentals of Solar Cells* (New York: Academic)
[16] Rau U 1999 Tunnelling-enhanced recombination in Cu(In,Ga)Se_2 heterojunction solar cells *Appl. Phys. Lett.* **74** 111–3
[17] Nadenau V, Rau U, Jasenek A and Schock H W 2000 Electronic properties of $CuGaSe_2$-based heterojunction solar cells. I. Transport analysis *J. Appl. Phys.* **87** 584–93
[18] Riben A R and Feucht D L 1966 Electrical transport in nGe-pGaAs heterojunctions *Int. J. Electron.* **20** 583–99
[19] Zohta Y 1973 Frequency dependence of C and $\Delta V/\Delta(C^{-2})$ of Schottky barriers containing deep impurities *Solid-State Electron.* **16** 1029–35
[20] Herberholz R, Igalson M and Schock H W 1998 Distinction between bulk and interface states in $CuInSe_2$/CdS/ZnO by space charge spectroscopy *J. Appl. Phys.* **83** 318–25
[21] Jasenek A, Rau U, Nadenau V and Schock H W 2000 Electronic properties of $CuGaSe_2$–based heterojunction solar cells. II. Defect spectroscopy *J. Appl. Phys.* **87** 594–602
[22] Walter T, Herberholz R, Muller C and Schock H W 1996 Determination of defect distributions from admittance measurements and application to Cu(In, Ga)Se_2 based heterojunctions *J. Appl. Phys.* **80** 4411–20
[23] Major J D, Proskuryakov Y Y and Durose K 2013 Impact of CdTe surface composition on doping and device performance in close Space sublimation deposited CdTe solar cells *Prog. Photovolt.* **21** 436–43
[24] Granata J E, Sites J R, Contreras-Puente G and Compaan A D 1996 Effect of CdS thickness on CdS/CdTe quantum efficiency *25th IEEE Photovoltaic Specialist Conf.*
[25] Hädrich M, Kraft C, Metzner H, Reislöhner U, Löffler C and Witthuhn W 2009 Formation of CdS_xTe_{1-x} at the *p–n* junction of CdS-CdTe solar cells *Phys. Status Solidi* C **6** 1257–60
[26] Rakhshani A E 2001 Heterojunction properties of electrodeposited CdTe/CdS solar cells *J. Appl. Phys.* **90** 4265–71
[27] Klenk R, Schock H W and Bloss W H 1994 Photocurrent collection in thin film solar cells and calculation and characterization for CuGaSe2/(Zn, Cd)S *Proc. 12th EU PVSEC* pp 1588–94
[28] McCandless B E and Sites J R 2002 *Handbook of Photovoltaic Science and Engineering* ed A Luque and S Hegedus (Chichester: Wiley) pp 21–30
[29] Durose K, Edwards P R and Halliday D P 1999 Materials aspects of CdTe/CdS solar cells *J. Cryst. Growth* **197** 733–42
[30] Proskuryakov Y Y, Durose K, Taele B M, Welch G P and Oelting S 2007 Admittance spectroscopy of CdTe/CdS solar cells subjected to varied nitric-phosphoric etching conditions *J. Appl. Phys.* **101** 014505